



Synthesis and characterization of chitosan/montmorillonite nanocomposites for application as edible coating

Camilly Aparecida Reis¹ , Mário Guimarães Júnior², Francys Kley Vieira Moreira³, José Manoel Marconcini⁴ and Livia Elisabeth Vasconcellos de Siqueira Brandão Vaz^{1,5*} 

Abstract

Edible coating can improve fruits shelf life and, consequently, reduce their waste. Chitosan, which presents a potential for chemical modifications and capacity to form films, can be an alternative for coating due to its biocompatibility, biodegradability, and antimicrobial properties. Chitosan film can be obtained through casting method presenting suitable mechanical properties, such as resistance to traction and elongation, ability to adhere to surfaces and selective permeability to gases, such as O₂ and CO₂. However, it is highly permeable to water vapor, which can limit its potential coating use. The properties of chitosan films can be improved through the formation of composites by inserting nanoclays as montmorillonite in the polymeric matrix. The objective of this study was to develop and characterize chitosan/montmorillonite nanocomposites for fruit coating aiming for future applications in the field of smart packaging. Nanocomposites were characterized by its microstructure, thermal, mechanical, and physico-chemical properties. X-ray diffraction analysis indicated changes in crystallinity with the insertion of montmorillonite. Nanocomposites became more transparent and significantly reduced its water permeability rate with 0.5% w/w montmorillonite addition. Elastic rigidity and tensile strength of the films were improved. Chitosan/montmorillonite nanocomposites demonstrated the potential to improve the storage time of Williams pears.

Keywords

Edible films, shelf life, nanoclay, biopolymer

Date received: 23 February 2021; accepted: 11 October 2021

Introduction

Edible coatings have shown potential in the conservation and increase of fruits shelf life. Their functions are to protect the fruits against mechanical, physical, and chemical damages and avoid the development of microorganisms. Materials used as coatings are biodegradable and edible as proteins, polysaccharides, lipids, or their combination (Dhall, 2013; Díaz-Montes and Castro-Muñoz, 2021; Jafarzadeh et al., 2021; Otoni et al., 2017;

Zambrano-Zaragoza et al., 2018; Zubair et al., 2021). Polysaccharides-based coatings are the most studied such

¹Programa de Pós-Graduação em Engenharia de Biomateriais, Universidade Federal de Lavras, Lavras, MG, Brazil

²Departamento de Eletromecânica, Centro Federal de Educação Tecnológica de Minas Gerais, Araxá, MG, Brazil

³Departamento de Engenharia de Materiais, Universidade Federal de São Carlos, São Carlos, SP, Brazil

⁴Laboratório Nacional de Nanotecnologia (LNNA), Embrapa Instrumentação, São Carlos, SP, Brazil

⁵Departamento de Engenharia, Escola de Engenharia, Universidade Federal de Lavras, Lavras, MG, Brazil

Corresponding author:

*Livia Elisabeth Vasconcellos de Siqueira Brandão Vaz, Departamento de Engenharia, Escola de Engenharia, Universidade Federal de Lavras, Lavras, Caixa Postal 3037, MG, Brazil.
Email: livia.brandao@ufla.br

as chitosan (CH) (Contreras-Oliva et al., 2012; Ojeda et al., 2021; Özdemir and Gökmen, 2017; Riaz et al., 2021; Sultan et al., 2021; Vieira et al., 2016), hydroxypropyl methylcellulose (Aman Mohammadi et al., 2021; Klangmuang and Sothornvit, 2018; Sousa et al., 2021; Vieira et al., 2020), pectin (Naqash et al., 2021; Panahirad et al., 2020; Priyadarshi et al., 2021), and carboxymethyl CH (Ali et al., 2021; Yaradoddi et al., 2020; Zhou et al., 2021).

CH is a biopolymer obtained from the deacetylation of chitin, which is one of the most abundant materials in nature, alongside lignin, after cellulose (Joseph et al., 2021; Kasaai, 2009; Måsson, 2021). Main source of chitin is the crustacean exoskeleton, but it can also be found in fungi, protozoa, green microalgae, and insects (Måsson, 2021; Van Den Broek et al., 2015). Chitin is a polymer linear chain composed of β -(1,4)-2-acetamido-2-deoxy-D-glucopyranose units, being highly acetylated and water insoluble (Måsson, 2021). CH chain is the result of chitin deacetylation process, formed by β (1,4)-2-amino-2-deoxy-D-glucopyranose units and has a deacetylation degree that varies from 70% to 95% (Kasaai, 2009; Måsson, 2021). This biopolymer is insoluble in the most common solvents, including water. Solubility is only possible at aqueous solutions with pH lower than its pKa, which varies from 5.5 to 6.5. At specific methods, such as acidic medium that presents low pH, amino groups ($-\text{NH}_2$) become protonated ($-\text{NH}_3^+$), causing an electrostatic repulsion among CHn molecules, weakening hydrogen interactions and favoring chemical-component interactions (Kaur and Dhillon, 2014; Kusmono and Abdurrahim, 2019; Pandey and Mishra, 2011). In addition, it possesses an antimicrobial property that is proportional to its degree of deacetylation (Ahmed et al., 2021; Amor et al., 2021; Fei Liu et al., 2001; Ke et al., 2021).

CH films show suitable characteristics for application as edible coatings on fruits by having great adhesion to surfaces, suitable mechanical properties, besides being biodegradable and nontoxic (Ahmed et al., 2021; Amor et al., 2021; Kaur and Dhillon, 2014; Ke et al., 2021; Kusmono and Abdurrahim, 2019; Måsson, 2021; Van Den Broek et al., 2015). However, is highly permeable to water vapor, which is an important and negative parameter for fruit coating (Elsabee and Abdou, 2013; Van Den Broek et al., 2015). Water vapor permeability and mechanical properties can be improved through the formation of nanocomposites by adding nanoreinforcements such as nanoclays (Bensalem et al., 2017; Chen et al., 2021; Giannakas et al., 2014; Hu et al., 2016; Pires et al., 2018).

Montmorillonite (MMT) is the most abundant clay mineral among smectites. MMT is formed by lamellae, which are composed of two layers of tetrahedral silica fused to a layer of octahedral aluminum hydroxide (Nagarajan et al., 2014). Its structure has continuity in axes *a* and *b* and has a parallel orientation in the (001) crystal planes, resulting in particle sizes that vary from 0.1 μm to 2 μm . Lamellae have an

irregular profile and can reach 100 nm diameter with ~ 1 nm thickness, which brings out a high aspect ratio (Merinska et al., 2002; Paiva et al., 2008). Between MMT layers, there are gaps, where exchangeable cations are found, such as Na^+ , in the case of sodium MMT, and also water molecules. The presence of these components compensates for the negative charge generated by isomorphic substitution on the lamellae and allows the formation of modified clays (Merinska et al., 2002). When MMT is dispersed in the polymer matrix, it forms nanocomposites with intercalated or exfoliated structures (Elsabee and Abdou, 2013). Because of the polycationic nature of CH, the interaction with MMT can be established through cation exchange and hydrogen bonds, promoting a strong interaction between both (Darder et al., 2003). This interaction is responsible for improving the mechanical properties of CHn film (Giannakas et al., 2014; Pires et al., 2018; Vlacha et al., 2016). Furthermore, MMT nanoplates dispersed in the matrix hind the diffusion of water vapor molecules, which decreases the film water vapor permeability (Bumbudsanpharoke et al., 2017; Giannakas et al., 2014; Lim et al., 2021; Pires et al., 2018; Rhim, 2011; Vlacha et al., 2016).

Although MMT has not been approved yet for food applications by the regulatory agencies, it is recognized as low toxicity material (Wang et al., 2008) and biopolymer/MMT nanocomposites have been applied as edible coatings (Cortez-Vega et al., 2014; Pinto et al., 2015; Pires et al., 2018; Rohini et al., 2020; Souza et al., 2019; Xu et al., 2018; Yan et al., 2019).

Therefore, the aim of this work was to develop and characterize CH/MMT nanocomposites for potential use as fruit coatings. As a possible application, the nanocomposites produced were applied to Williams pears (*Pyrus communis*) and their weight loss and visual appearance were evaluated. This fruit is climacteric and shows an increase in its respiration rate, ethylene production, and weight loss by respiration and transpiration at postharvest period that contributes to its short shelf life (Chitarra and Chitarra, 2005). These kinds of fruits have a smooth and shiny surface which could present high wettability or the presence of surface charges. Thus, a strong interaction between coating and fruit peel is required to achieve a good surface coverage. Li et al. (2012) showed that CH coating on Yali pears delayed the senescence induced by bruise damage of the fruits.

In this sense, CH/MMT nanocomposites that combine hydrophilic behavior, improved barrier, and mechanical properties are being proposed to be studied as candidates for pears coating.

MATERIAL AND METHODS

Material

Materials used were CH with medium molecular weight and 86.7% deacetylation degree (Polymar, Brazil), sodium

MMTe (Southern Clay Products, USA), and acetic acid (Sigma Aldrich, Brazil). Williams pears (*Pyrus communis*) were purchased at the local market.

Elaboration of nanocomposites films

The synthesis of nanocomposites started by adding 1.0% w/w CH in acetic acid solution (1.0% v/v) followed by homogenization at an Ultra-Turrax mixer (IKA T25, Germany) at 1000 rpm for 5 min. Then, the prepared solution was centrifuged at 10000 rpm during 10 min to remove any insoluble material. Separately, the adequate concentrations of MMT were dispersed in acetic acid solution (1.0% v/v) and subjected to a probe sonicator (Branson, USA) for 10 min at 40 W. This dispersion was added to CH solution and sonicated for 5 min at 40 W. Films were formed by casting and spreading its solution on nonstick plates, followed by drying step at 30 °C for 24 h. Nanoclay concentrations used were 0.5% w/w (MMT-0.5), 1.0% w/w (MMT-1), 2.0% w/w (MMT-2), and 4.0% w/w (MMT-4) based on CH weight. A film composed exclusively by CH was developed for comparison purposes.

Characterization of nanocomposites

Scanning electron microscopy (SEM). The morphology of the films produced was observed under an SEM microscope JSM 6510 (JEOL Ltd, Japan), operating at 10 kV. The analysis was carried out on the top surface and on the cross-section surface of the films, after fracture by liquid nitrogen bath. Both surfaces were submitted to gold metallization.

Energy dispersive spectroscopy (EDS) was performed for MMT-0.5 to evaluate the chemical composition of the agglomerations observed.

Fourier transform infrared spectroscopy (FTIR). FTIR spectra were obtained with a Vertex 70 spectrometer (Bruker, Germany) by attenuated total reflectance mode (ATR), at room temperature. The spectra were measured in the range of 400 cm^{-1} – 4000 cm^{-1} , with a resolution of 4 cm^{-1} . FTIR was used to evaluate the chemical interactions between CH and the nanoclay.

X-ray diffraction (XRD). Powder XRD measurements were performed on the obtained film samples using a LabX XRD-6000 diffractometer (Shimadzu, Japan) operating with Cu- K_{α} radiation (1.5428 Å), at 30 kV, 30 mA. The diffraction intensity was detected in the 2θ range from 3° to 30°, at a scan rate of 1°/min.

Bragg's law (equation (1)) (Bragg, 1912; Bragg et al., 1913) was used to evaluate the possible process of intercalation between CH chains and MMT lamellae, by

calculating the distance between nanoclay layers.

$$n\lambda = 2d \sin \theta \quad (1)$$

where “n” is the diffraction order equal to a whole number of wavelength (1 was used); “ λ ” is the length of monochromatic radiation (Cu- K_{α} radiation); “d” is the interplanar distance in a given structure (basal spacing); and “ θ ” is the Bragg diffraction angle.

Thermal analysis. Thermogravimetric analysis (TGA) and differential scanning calorimetry (DSC) were performed. The effect of MMT addition on thermal stability of CH was analyzed by TGA. The measurements were performed with a Q500 (TA Instruments, USA) thermoanalyzer. Samples of 5 ± 1 mg were heated from room temperature to 600 °C at a rate of 10 °C/min, using synthetic air at a rate of 60 mL/min. The dynamic thermal behavior of the samples was analyzed using heat flow DSC. The measurements were performed with Q100 (TA Instruments, USA) calorimeter from room temperature to 300 °C at a rate of 10 °C/min, using nitrogen gas at of 60 $\text{mL}\cdot\text{min}^{-1}$.

Film thickness. The thickness of nanocomposites produced was measured with a micrometer (IP65, Mitutoyo) at 10 points randomly chosen. The mean values were calculated and used to evaluate the mechanical properties.

Water solubility. Gontard et al., 1994 methodology was adapted for water solubility measures. Samples of 2 cm diameter were dried at 55 °C for 24 h. After this period, the initial weight was measured, and the samples were submerged in 30 mL of distilled water for 24 h. Subsequently, the samples were dried again at 70 °C for 24 h. After this process, the insoluble material weight was determined, and the results were expressed as percentage in relation to the initial weight.

Water vapor permeability rate (WVPR). Gravimetry using ASTM-E-96-00 (ASTM, 2000b) took place to determine WVPR. Amber recipients with perforated caps were used as permeability cells. These cells contained silica gel and circular specimens of 10.6 mm diameter were placed between the recipient and caps. Cells were placed at hermetic desiccators containing distilled water at 19 ± 1 °C for 240 h. Every 24 h, weight gain measures were performed (Guimarães et al., 2015). WVPR was estimated by linear regression between weight gain (g) and time (days). The slope of this curve corresponds to the amount of water vapor diffusing through the film. The determination was made according to equation (2) and the result expressed in $\text{g}/\text{m}^2\cdot\text{day}$ (Guimarães et al., 2015).

$$\text{WVPR} = \frac{g}{t \times A} \quad (2)$$

in which “g/t” corresponds to the slope of the line obtained by linear regression between weight gain (g) and time (days) and “A” is the permeation area of each specimen (m²).

Water vapor permeability was calculated from equation (3) and was expressed in units of g.mm/KPa.h.m² (Guimarães et al., 2015).

$$WVP = \frac{WVPR \times e}{ps \times \left(\frac{Hr}{100}\right) - ps \times \left(\frac{Hri}{100}\right)} \quad (3)$$

in which “WVPR” is the water vapor permeability rate (equation (1)); “e” is the specimen thickness (mm); “Hr” is the relative humidity inside the desiccator containing water (100%); “Hri” is the relative humidity inside the permeation cell containing silica gel (0%) and “ps” is the water vapor saturation pressure (KPa) at test temperature (T), which was calculated by equation (4) (Tetens, 1930).

$$ps = 0.6108 e^{\frac{17.27 \times T}{T+237.3}} \quad (4)$$

The evaluation of this property was extremely important to define the optimal nanoclay concentration that should be used for the application desired.

Mechanical properties. Mechanical properties were performed at a DL 3000 (EMIC, Brazil) universal testing machine. Tensile strength and Young modulus were calculated according to ASTM D882-09 (ASTM, 2000a). 10 specimens of each treatment, with 15 mm width and 100 mm length, were submitted to traction test at 10 mm/min speed with 10 kgf charge. The tensile strength calculation was made through the ratio between maximum force and the cross-section area of the specimen. The elastic modulus was calculated from the slope at the linear region of the stress *versus* strain curve measured.

Wettability and surface energy. Surface properties of nanocomposites and pears were estimated by contact angle measurements using the sessile drop method at a Krüss DSA25E (Krüss, Germany) goniometer. Samples of 1 cm width and 4 cm length were measured and, for the pear surface, an epicarp piece was cut very carefully. Distilled water was used as drops and the contact angle was measured after 2 s of contact between the sample and the drop. Surface energy was performed by Owens, Wendt, Rabel and Kaelble (OWRK) method using the Advance-Drop Shape software for three different solvents.

Optical properties. Optical transmittance of nanocomposites was measured in a UV-VIS Lambda 25 (Perkin Elmer, USA) spectrophotometer, with a double-beam of tungsten and deuterium source and accuracy of 0.1 nm. Film samples were cut and placed directly on the equipment.

Measurements were performed using the transmittance mode at the range of 400 to 700 nm.

Williams Pears coating

From water permeability rate results, 0.5% w/w MMT concentration was defined as the ideal concentration to be used for nanocomposites formulation.

Coating solutions were prepared using the same methodology previously proposed, using CH and 0.5% w/w of nanoclay. First, pears were sanitized in a sodium hypochlorite solution (100 ppm) for 20 min. For coating, Williams pears were immersed into the coating solution for 2.5 min followed by drying stage for 1 h at room temperature. In the second step, to guarantee a uniform coating of the entire surface, the immersion procedure was repeated followed by the drying stage overnight at room temperature.

After the drying process, both coated and uncoated pears (control – C) were stored at room temperature, for 15 days. During these days, every 24h, all pears underwent visual inspection and weight loss control to verify the possible success of the developed methodology. The results were expressed in percentage in relation to the initial weight of pears.

Statistical analysis

The software Sisvar 5.0 (Ferreira, 2015) was used for statistical analysis of data obtained. The Scott-Knott test was applied to evaluate significant differences among the treatments developed.

RESULTS AND DISCUSSION

Characterization of nanocomposites

Scanning electron microscopy (SEM). The top surface of CH film showed up quite homogeneous, while the surfaces of nanocomposites presented heterogeneous characteristics. From 0.5 to 2.0% w/w MMT concentrations, the top surface did not show significant morphological modifications. For MMT-4, the heterogeneity was quite evident and detectable. It was possible to observe the coexistence of different phases, those containing only CH and others containing dispersed MMT (Figure 1).

By analyzing the fracture surfaces, it could be observed a homogeneous morphology for CH film while for MMT-0.5, MMT-2, and MMT-4 nanocomposites agglomerates could be detected, indicating a heterogeneous morphology. These clusters are particles and lamellas of MMT dispersed into the CH matrix that increases in quantity with the increase of MMT concentration (Figure 1 (e) to (g)).

To elucidate the chemical nature of agglomerations, energy dispersive spectroscopy (EDS) was performed at different regions that presented clusters. MMT general formula is M_x (Al_{4-x}Mg_x) Si₈O₂₀(OH)₄, with M being

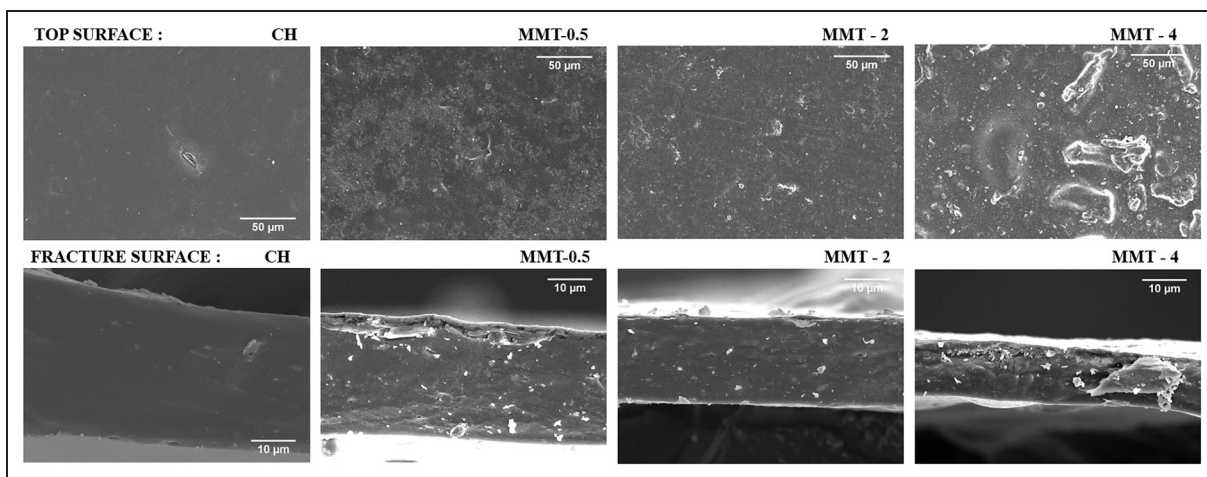


Figure 1. SEM micrographs from top and fracture surfaces of CH, MMT-0.5, MMT-2, and MMT-4. CH; chitosan; MMT: montmorillonite; SEM: scanning electron microscope.

the exchangeable cation (Santos, 1989). MMT spectrum measured corroborates all its characteristic elements (Figure 2(a)), with Na being the exchangeable cation. Si, O, Mg, Al, Fe, and Ca peaks appeared with low intensity, indicating its low concentration. In addition, it may also indicate that these elements could be present in the form of exchangeable cations both in the gallery and on the surface of the clay (Paiva et al., 2008). The prominent peak of carbon is related to the support material used to perform the analysis. For nanocomposites, it was possible to detect both CH and MMT elements. Si, Mg, and Al refer directly to clay while N refers directly to CH. Other elements as C and O refer both to CH and to MMT. To illustrate, Figure 2b shows the spectrum obtained for treatment with lower concentration of nanoclay (MMT-0.5). Through this spectrum, it could be seen that even for low concentrations of clay used within the polymer matrix, it was possible to detect its characteristic elements.

The results obtained from the measured spectra could be corroborated through the elemental chemical maps obtained for MMT-0.5 fracture surface (Figure 2(c)) and through the elementary ratio calculations for MMT and MMT-0.5 (Table 1) at the cluster region. It is evident through the chemical maps the increase in the concentration of typical clay elements at agglomerates regions, such as Si, Al, and O and its reduction in other regions.

Fourier transform infrared spectroscopy (FTIR). FTIR was applied to verify which vibrational modes were possible to be obtained after the nanocomposites synthesis. From the analysis of the spectrum obtained for CH film produced free of clay, it was possible to observe bands in the region of 3200 cm^{-1} and 2900 cm^{-1} , which are characteristics of hydroxyl group (OH) and CH bonds, respectively (Figure 3). Other CH characteristics bands at 1640 , 1540 , and 1400 cm^{-1} , assigned to the presence of carbonyl

group ($\text{C}=\text{O}$), amino group (NH_2) and carboxyl group ($-\text{COO}-$), respectively, were detected. Also, it was possible to observe bands at 1150 , 1070 , and 1015 cm^{-1} that correspond to CO bonds (Pranoto et al., 2005).

The morphological analyzes of the nanocomposites confirmed the presence of clay chemical elements in its structure and highlighted the formation of agglomerates, related to clay particles and lamellae, which increase in concentration with the increase of the amount of MMT added to the polymer matrix. Through the analysis of the spectra obtained for the nanocomposites, the typical CH vibrational modes are evidenced. It was expected since it is in greater proportion in the composite (Figure 3). However, the evidence of the interactions between clay and CH can be perceived, even if in a subtle way, through a slight displacement of the OH band (3200 cm^{-1}) and amino bands (1540 cm^{-1}) for larger wavenumber values when MMT was added. It is also noticed that as MMT contraction increases, more displaced those bands become. It may occur due to intermolecular bonds between hydroxyl and amino groups of CH chains with MMT OH, which tends to facilitate the intercalation of MMT lamellae. This behavior has already been observed in other studies (Darder et al., 2005; Fiori et al., 2014; Hu et al., 2016; Lavorgna et al., 2010) and corroborates the results obtained by SEM/EDS. It is possible that the nanocomposite production process promotes the intercalation and exfoliation of the clay layers. This can be made clearer through XRD analysis.

Another fact that could be observed was a slight change in the vibrational modes related to the carboxyl group band (1400 cm^{-1}). Also, a slight widening could be perceived for the carbonyl group band (1070 and 1015 cm^{-1}), as well as an increase in the intensity of the band close to 1000 cm^{-1} as the concentration of MMT increases. These alterations may be related to the occurrence of typical MMT bands at 990 cm^{-1} related to SiO bond and around 840 and 726

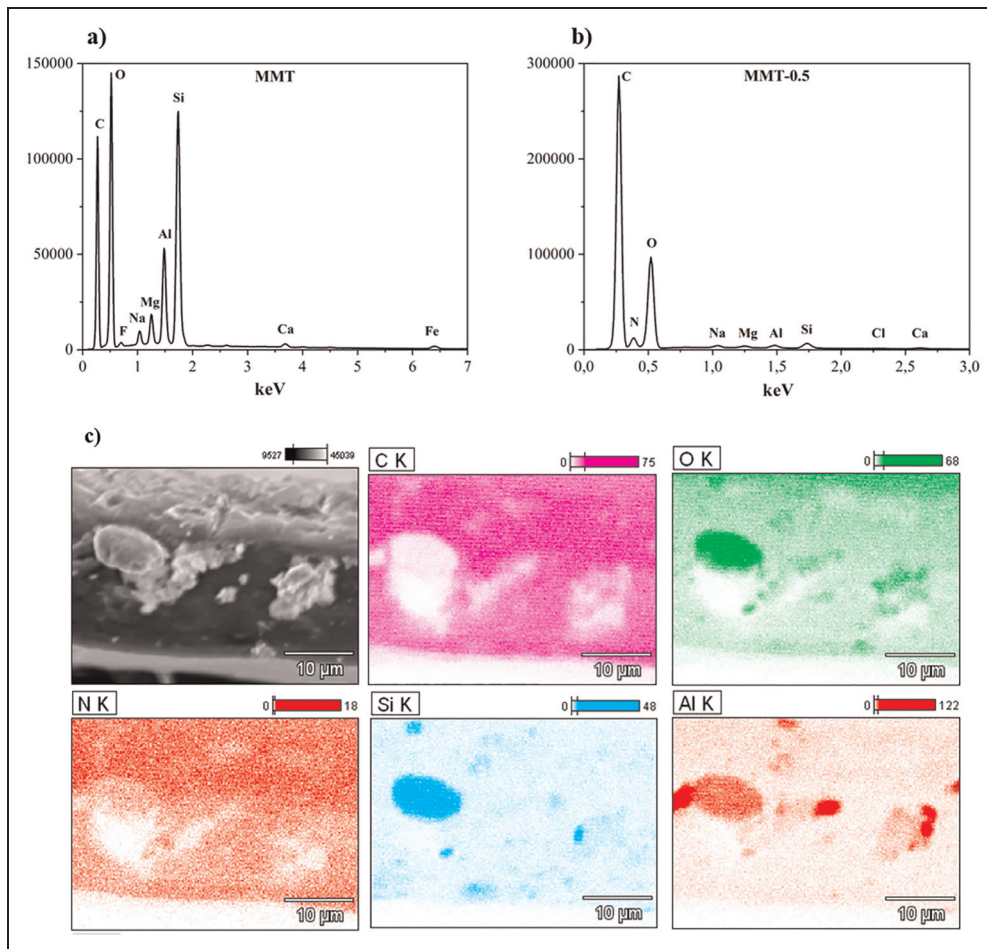


Figure 2. (a) MMT and (b) MMT-0.5 EDS spectra. (c) MMT-0.5 EDS elemental chemical maps. EDS: energy dispersive spectroscopy; MMT: montmorillonite

Table 1. Comparative EDS elemental ratios (wt%) for MMT and MMT-0.5.

Element	MMT (wt%)	MMT-0.5 (wt%)
C	27.91	35.02
N	0.00	15.39
O	43.33	35.04
F	0.00	0.00
Na	1.23	0.81
Mg	1.95	0.80
Al	5.93	2.83
Si	16.93	3.98
P	0.06	0.00
S	0.11	0.16
Cl	0.11	0.87
K	0.00	0.10
Ca	0.56	3.31
Ti	0.15	0.24
Fe	1.72	1.44
	100.00	100.00

EDS: energy dispersive spectroscopy; MMT: montmorillonite.

cm^{-1} related to (Al, Mg) OH (Günister et al., 2007). These are indicative that, in fact, the interaction between biopolymer and clay has taken place and that an improvement at mechanical and barrier is possible.

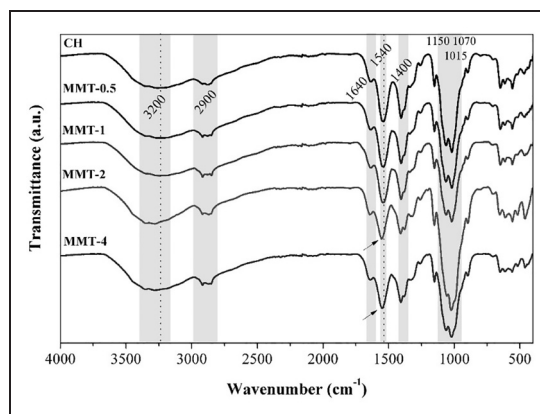


Figure 3. FTIR spectra of CH and nanocomposites. CH: chitosan; FTIR: Fourier transform infrared spectroscopy.

3.1.3 X-ray diffraction (XRD). FTIR data suggest a possible clay intercalation or exfoliation process when producing nanocomposites. Through XRD it was intended to elucidate this aspect, confirming the type of interaction established between CH chains and MMT lamellae. In addition, the nanocomposites crystallinity was evaluated.

CH film exhibited diffraction peaks around 10° , 18° , and 22° , related to (020), (110), and (120) crystallographic planes, respectively (Figure 4). The position and intensity of these peaks, in particular (020) and (110), directly depend on the degree of deacetylation of the polymer (Anusha et al., 2016; Giannakas et al., 2014; Jampafuang et al., 2019; Mogilevskaya et al., 2006; Rhim et al., 2006; Wang et al., 2005; Zhang et al., 2005). The higher this degree, the lower the intensity of the peaks, and more accentuated are the shift toward greater angles. This could be observed and was expected, since the degree of deacetylation of the CH used was 86.7%. Furthermore, it was also notable that the increase in MMT concentration influences the intensity and width of these characteristic peaks. It was possible to observe a decrease in the intensity of these peaks, also related to the degree of deacetylation of CH, as well as their widening as the concentration of MMT increased. Thus, in accordance with the SEM morphology results, the addition of MMT in CH films promotes a decrease in crystallinity of the films, confirming the occurrence of interaction between the materials that compound the nanocomposites, as indicated by FTIR analysis and observed by other researchers (Chen et al., 2021; Lavorgna et al., 2010; Pires et al., 2018). It may be observed that as the MMT concentration increases, more amorphized the nanocomposite film became.

From the MMT diffractogram, it was possible to observe the peak of (001) crystallographic plane, approximately at 6.6° , which corresponds to the basal spacing of 1.33 nm (Figure 4). The (001) crystallographic plane of MMT can be expanded by the insertion of molecules between clay

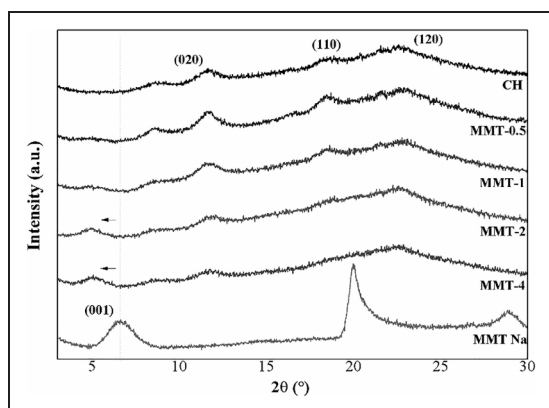


Figure 4. MMT, CH and nanocomposites diffractograms. CH: chitosan; MMT: montmorillonite.

lamellae (Paiva et al., 2008; Ramadan et al., 2010). When combining MMT with CH, this peak shifted to smaller angles for MMT-2 and MMT-4 indicating an increase in the clay basal space. For MMT-2 treatment, this increase was of 0.46 nm while for MMT-4, was of 0.42 nm. This increase of the basal spacing for high concentrations of MMT confirms the hypothesis of the occurrence of an intercalation of clay structure with CH chains when synthesizing the nanocomposites, thus elucidating the results obtained by SEM and FTIR.

For lower MMT concentrations, the peak relative to (001) crystallographic plane were not evidenced, which suggests the occurrence of disordered intercalated clay structure or probably exfoliated structure (Pereira et al., 2017; Wang et al., 2005).

Thermal properties. From TGA, it was observed three significant degradation stages for CH film as for nanocomposites (Figure 5(a)). The first stage detected was in the range of 25°C – 130°C that is associated to water evaporation. The second stage detected between 130°C and 180°C is related to degradation and deacetylation of CH, remaining 40% of solid residue. The third one, at higher temperatures (400°C – 550°C), corresponds to an oxidative degradation of the carbonaceous residues that were originated at the second weight loss.

CH presented the greatest weight loss during the second stage, as demonstrated by the first derivative of the thermogravimetric curve. It was possible to attest that nanocomposites showed greater thermal stability than CH film, as their weight loss occurred more slowly. This can be explained by the formation of carbon–silicate multilayers structures after pyrolysis, which maintains the clay structure even at high temperatures. These structures can accumulate on the material surface and, consequently, prevent the release of volatile substances formed during the thermal process (Bumbudsanpharoke et al., 2017; Darder et al., 2003; Hu et al., 2016; Silvestre et al., 2011; Wang et al., 2005). The peak deviation for low temperatures of MMT-1 confirms the reduction of the structural stability promoted by clay addition. This reduction in temperature may be related to a heterogeneous dispersion of silicate tactoids in the polymeric matrix and to a lower degree of intercalation that could be observed from XRD analysis (Figure 4). Contrarily, the increase in the degradation temperature for MMT-2 and MMT-4 could be related to higher degree of intercalation. Evaluating the decomposition temperature that promoted 50% of mass loss, it was observed that there was an increase in this temperature with the addition of MMT. For MMT-4, the increase reached 40°C . In this case, the confinement of polymer chains within the clay layers tends to slow down the movement of the matrix chains, resulting in an increase of thermal stability. These results corroborate what was observed by XRD and FTIR analysis.

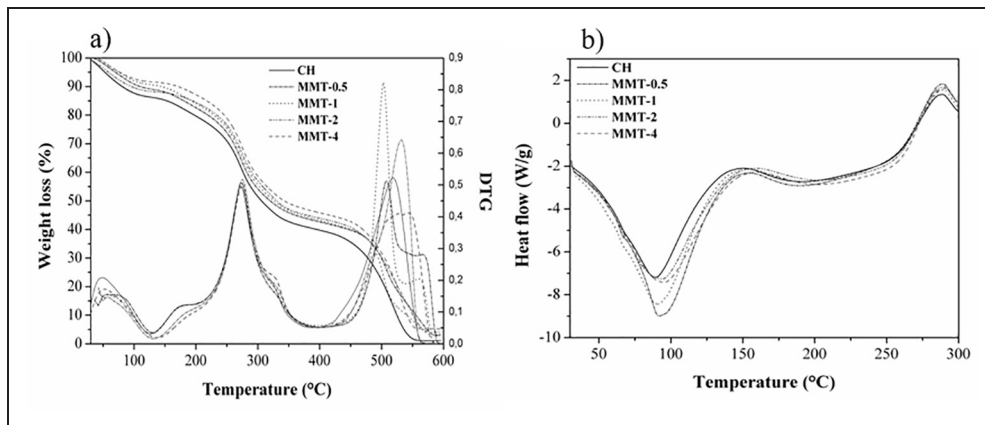


Figure 5. (a) TGA and (b) DSC curves for CH and nanocomposites. CH; chitosan; DSC: differential scanning calorimetry; TGA: thermogravimetric analysis.

DSC analysis showed the presence of two endothermic peaks for CH (Figure 5(b)). The peak at approximately 89 °C is related to solvent evaporation (acetic acid), which depends on the drying process of the sample before the test, while the peak at approximately 189 °C is related to CH crystallization (Casariego et al., 2009).

When MMT is added, it could be seen that there was a slight shift to higher temperatures for the first endothermic peak, that is, solvent evaporation occurs more slowly. The increase in thermal stability with the addition of particles can be attributed to a decrease in the diffusion of volatile compounds through the material as attested by TGA. The same fact could be observed for peaks related to CH crystallization, with a shift to higher temperatures for nanocomposites, showing that there was a change in the CH crystallization kinetics with the addition of MMT.

The exothermic peak around 288 °C corresponds to the decomposition of the amino groups of CH. In one scan DSC analysis, the same behavior was observed by other researchers (Casariego et al., 2009; Martínez-Camacho et al., 2010)

So, it was possible to verify that CH film lost solvent more easily than nanocomposites. As the MMT concentration increases, higher temperature for removing the solvent

is required, since the shift of endothermic peak occurred from 89 °C for CH to 95 °C for MMT-4. Ultimately, these results suggest that nanocomposites present greater solvent retention capacity and better thermal stability.

Film thickness. The thickness values measured were 0.037 mm for CH, 0.038 mm for MMT-0.5, and 0.039 mm for MMT-1, MMT-2, and MMT-4. Despite the formation of nanoclay agglomerates, they present themselves quite small (< 3 μm) and the thickness was not directly influenced by them. There were no significant differences observed among treatments. It can be affirmed that, on average, all films presented the same thickness.

Water solubility. The percentage of soluble matter in the CH film was 28.6% (Table 2). MMT addition promoted a decrease in water solubility with a significant difference ($p < 0.05$) for clay concentrations of 2.0% and 4.0% w/w. This fact is explained by the distribution of clay plates in the matrix, which form strong interactions such as hydrogen bonds with CH chains, demonstrated by FTIR spectra and XRD patterns. Thus, it is not possible for water molecules to break these bonds, which results in the reduction of water solubility of the films. This same behavior has also

Table 2. Water solubility, water vapor permeability rate (WVPR), Young’s modulus, tensile strength, and elongation at break of nanocomposites.

Samples	Water solubility (%)	WVPR (g/day.m ²)	Young’s modulus (MPa)	Tensile strength (MPa)	Elongation at break (%)
CH	28.6 (0.7) ^a	33.8 (0.2) ^c	1149 (144) ^a	21.4 (1.6) ^a	0.025 (0.004) ^a
MMT-0.5	26.3 (0.7) ^a	28.6 (0.4) ^a	2125 (141) ^b	25.8 (1.9) ^a	0.068 (0.007) ^c
MMT-1	27.1 (1.1) ^a	30.4 (1.0) ^b	2108 (105) ^b	25.3 (1.4) ^a	0.033 (0.009) ^b
MMT-2	24.2 (0.3) ^b	31.0 (0.1) ^b	2233 (212) ^b	33.5 (4.1) ^b	0.033 (0.009) ^b
MMT-4	24.2 (1.7) ^b	27.9 (0.6) ^a	2173 (174) ^b	30.8 (3.3) ^b	0.021 (0.006) ^a

Standard deviation is given in parentheses. CH: chitosan; MMT: montmorillonite.

been reported by other authors that worked with MMT and CH (Beigzadeh Ghelejlou et al., 2016; Casariego et al., 2009; Souza et al., 2018).

Water vapor permeability rate (WVPR). CH/MMT nanocomposites showed a significant decrease ($p < 0.05$) for WVPR (Table 2). It could be observed that there was a decrease in the WVPR for nanocomposites. This decrease is expected due to the tortuous path formed by the nanoplates distribution in the polysaccharide matrix and to the strong interactions between nanoclay structure and CH chains, which hinders the passage of water vapor molecules (Rhim, 2011). However, MMT-4 did not differ statistically from MMT-0.5. Possibly, due to the formation of clay exfoliated structure for the lowest nanoclay concentration instead of the intercalated structure detected for MMT-4, as suggested by XRD analysis. Interactions between MMT and CH chains have also been observed by FTIR spectra (Figure 3). Furthermore, the SEM results showed the distribution of MMT lamellae across polymeric matrix, hindering the mobility of water vapor molecules through the film.

Decreasing in WVPR has also been observed by other researchers that worked with MMT and CH (Beigzadeh Ghelejlou et al., 2016; Giannakas et al., 2014; Vlacha et al., 2016).

This property is particularly important for the coating process because during postharvest, fruit weight loss is related to the water vapor loss through transpiration. One manner to decrease the weight loss is to increase the water vapor barrier of the coating. Thus, considering only WVPR results, MMT concentrations of 0.5% and 4% w/w were statistically equal, and the lowest concentration would be ideal for coating process, because it could minimize possible interactions between nanoclay and the fruit or even its migration. In addition, it reduces the cost production.

Mechanical properties. As expected, Young's modulus of nanocomposites increased if compared to CH (Table 2), but there is no proportionality with the increase in clay concentration. The resistance elastic deformation depends not only on the MMT concentration but also on its distribution into the polymer structure. Nanoclays distribution occurred heterogeneously in the CH film, giving rise to clusters as could be seen in the microstructure (Figure 1). These ceramic agglomerates offer great resistance to elastic deformation due to the nature of the silicate bonds. Therefore, the transmission of stresses along the composite structure becomes difficult, resulting in a high Young's modulus.

For tensile strength, only MMT-2 and MMT-4 showed a significant increase compared to CH. With 0.5% w/w MMT addition, it was possible to obtain a more ductile film, that is, with a high elongation at break. This is due to the low

concentration of the mechanical reinforcing agent, contributing to the deformation process. Once the MMT concentration is further increased, a decrease of the elongation at break can be perceived, that is, there is an increase in the resistance to deformation due to an increase in the concentration of available reinforcing agents. However, MMT-4 did not show a significant difference related to CH. Possibly, this is due to accentuated intercalation between clay lamellae and CH chains. When comparing the results of MMT-2 and MMT-4, a clear difference could be noticed. Doubling the concentration of reinforcing agents in the nanocomposite promotes an increase in restrictions to dislocations movement, which end up accumulating in certain microregions originating tension points that turned the material more fragile than plastic and, directly contributed to a considerable increase of the elastic modulus and, therefore, decrease of tensile strength and of elongation at break.

In a general analysis, the improvement of the mechanical properties could be attested and is related to the strong interactions between the intercalated/exfoliated MMT lamellae and the polymeric chains by hydrogen and electrostatic bonds. This relation has also been reported by other researchers (Bumbudsanpharoke et al., 2017; Chen et al., 2021; Kusmono and Abdurrahim, 2019). Additionally, it can also be ascribed to the mechanical strength of the clay itself due to its high surface area, aspect ratio, and elastic modulus (Alexandre and Dubois, 2000; Pandey et al., 2005; Pavlidou and Paspaspyrides, 2008).

Contact angle measurement. Fruits surfaces that present hydrophilic behavior establish strong interactions with hydrophilic coatings in function of the good chemical and physical affinity between such surfaces (Assis and Britto, 2014). From contact angle measurements, it was possible to determine the kind of surface behavior of the nanocomposites besides CH and Williams pears surface. Pears and CH showed up hydrophilic behavior since the measured contact angle was of $79.7 \pm 2.1^\circ$ and $83.7 \pm 0.9^\circ$, respectively. This demonstrates that there is a chemical and physical affinity between CH film and pear surface, indicating a great possibility of success for the coating. Addition of 0.5% w/w MMT did not significantly affect the contact angle of the film produced, which presented the value of $85.3 \pm 0.5^\circ$. Therefore, CH/MMT film has great potential for uniformly coating the surface of pears, due to the chemical affinity between the surfaces.

Pear surface presented a surface energy of 29.0 ± 4.5 mN/m, similar to the values obtained for the films which reached 24.6 ± 3.8 mN/m (CH) and 25.8 ± 6.2 mN/m (MMT-0.5). This corroborates the results demonstrated by contact angle measures and, together with the microstructural and mechanical results, confirms the great potential of success for the coating.

Optical transmittance. Last but not least, for the coating step, the optical transmittance must be evaluated, since the fruits appearance cannot be changed, and the addition of clays can affect it.

The best result obtained was for MMT-1 (Figure 6). MMT-4 also showed improvement, but less than MMT-1 and higher than MMT-0.5. This indicates that the internal structure of the nanocomposites, related directly to the clay concentration, is responsible for the passage of light through the film. As for MMT-2 and MMT-4, there was an intercalation between the clay lamellae and the polymer chains, this generated a greater obstruction to the passage of light, resulting in an absorption and reflection of it. The result obtained for MMT-0.5 is related to the clay exfoliation organization, as detected through other analysis techniques, which facilitated the passage of light as there are not as many strong interactions between the polymer matrix and clay chains, as occurs for MMT-2 and MMT-4. Through this result, the addition of 1.0% w/w MMT is the best concentration for a structural organization that allows greater light passage, possibly because it presents regions of intercalation and clay exfoliation throughout the entire composite. In the case of MMT-2, is believed that the developed analysis has reached a region with many clay clusters with a larger size. That implied in a greater scattering of light across the film. According to Zeng et al., 2005, when clay lamellae are well distributed over the polymeric matrix, the transparency of the film is not affected, because the particles are smaller than the wavelength of visible light.

Ultimately, it is necessary to verify the specific behavior of the film with 0.5%w/w MMT, since that was the defined optimal concentration for the pear coating. Although MMT-0.5 did not present the best transmittance result, it offered a considerable increase in light passing through the film when compared to CH. Therefore, it can be

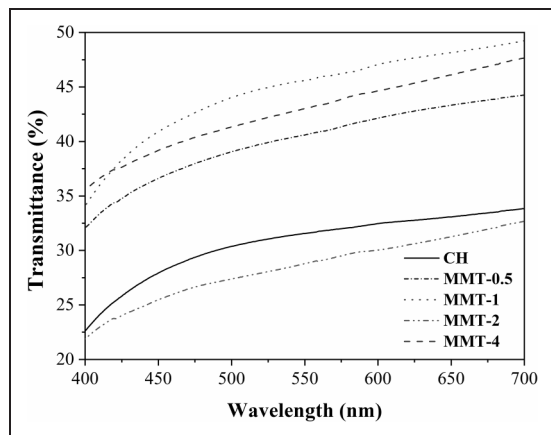


Figure 6. Transmittance of nanocomposites in the range of 400–700 nm.

affirmed that the MMT-0.5 film is suitable for coating fruit surfaces.

Williams pears coating

After the characterization of the nanocomposites, MMT-0.5 was chosen for the stage of the preliminary coating tests. To recap, this treatment presented a microstructure without large size clusters, low solubility in water, possible exfoliated structure, low WVPR, suitable mechanical properties, chemical affinity to pears, and adequate light transmittance. In addition, it was the lowest amount of clay used, which reduces production costs and minimizes possible migration into the fruit.

In fact, as expected, after the analysis of mechanical and surface properties, a homogeneous coating of the fruit was possible, without cracking, blistering, or bubbles formation. The aim of this work was to develop nanocomposites with ceramic reinforcement agents that could be used for the purpose of coating fruits to reduce their losses by increasing their shelf life. Once the interactions between the composite components and their direct effect on the structure of the nanocomposites were investigated, as well as the properties that would claim to be possible or not a pear coating with the films produced, it was decided to preliminarily evaluate the effect of the optimal treatment to the weight loss of pears.

Weight loss. An important parameter to evaluate the shelf life of fruit is the weight loss, which is the result of the combined respiration and transpiration processes (Chitarra and Chitarra, 2005). Weight loss of the Williams pears is shown in Figure 7.

In the first nine days of storage, no changes could be observed among the treatments. After 12 days, a differentiation started to be notable. It was possible to observe that

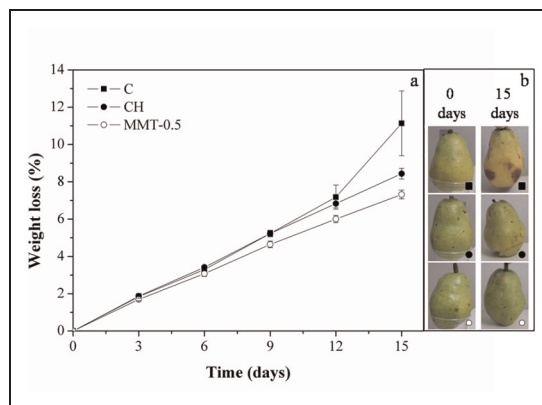


Figure 7. (a) Weight loss of Williams pears during 15 days of storage and (b) visual comparison of the treatments C (control), CH, and MMT-0.5. CH: chitosan; MMT: montmorillonite.

even with the increase of the weight loss, for the pear coated with the nanocomposite, this increase was reduced. After 15 days of storage, a sharp increase in weight loss could be observed for the control group while coated pears (CH and MMT) showed less impact. Moreover, the result presented by MMT-0.5 was better than that of CH. As previously observed, MMT-0.5 presented lower WVPR than CH film, and the weight loss is related to the loss of water vapor through transpiration. Moraes et al., 2012 observed the same behavior when studying Williams pears coating with alginate and carrageenan, in which there was a prominent difference in weight loss after 10 days of storage at 25 °C.

Just out of curiosity, from visual comparison of the treatments (Figure 7(b)), the control group exhibited a visual change in the color of the pears, modifying from green to yellow in the first 5 days of storage while the coated fruits remained unmodified. The incidence of deterioration, mainly characterized by the appearance of visible fungi, showed that at the end of 15 days of storage, 60% of the control pears showed signs of this contamination. For coated pears with CH, 20% were contaminated by fungi, while those coated with MMT-0.5, did not show visible contamination. It was possible to see the degree of degradation of coated and uncoated fruits after 15 days (Figure 7(b)), however, further analysis should be performed to check other qualities attributes of pears during storage, as mentioned before.

CONCLUSION

In this work, the elaboration of CH/MMT nanocomposites with different clay additions (0.5 to 4 w/w%) was proposed, as well as the study of their structure, interactions between the composite components and analysis of properties to elaborate a suitable material for Williams pears coating. For this, a composite that combines hydrophilic behavior, improved barrier, and mechanical properties are most suitable.

The top and fracture surfaces of the films produced had their morphology analyzed. It was possible to detect heterogeneities only on the top surface of MMT -4, while the fracture surfaces showed the formation of micrometric agglomerates that increased in quantity as the concentration of clay added to the polymer matrix also increased. EDS analyzes confirmed the chemical composition of clay for these agglomerates, which are particles and lamellas of MMT dispersed into CH matrix. An interaction between MMT and CH chains was observed by FTIR spectra by (i) a displacement of the hydroxyl amino bands with the addition of MMT, (ii) changes detected on the vibrational modes related to the carboxyl and carbonyl group band, and (iii) alterations in the intensity of the band close to 1000 cm^{-1} as the concentration of MMT increases. These modifications are related to intermolecular bonds between

hydroxyl and amino groups of CH chains with MMT OH, besides the presence of typical MMT bands that directly influenced the spectra. From XRD analysis, it was possible to detect an increase in the basal spacing for high concentrations of MMT, and along with FTIR results, it could be confirmed the occurrence of an intercalation of clay structure with CH chains for nanocomposites with higher MMT concentrations while for lower ones an occurrence of exfoliated structure.

These microstructural changes were also possible to be observed and proven through optical transmittance and mechanical analysis. MMT-2 and MMT-4 films, that presented an intercalated structure, were more absorbing/reflecting of light than MMT-0.5 or MMT-1. The structural organization of reinforcement agents within the polymer matrix, as well as the interrelationship between the composite components directly influenced the mechanical properties, resulting in an improvement of Young's modulus, tensile strength, and elongation at break when compared to CH.

Nanocomposites also proved to be more thermally stable, showed low water solubility and a greater barrier to water vapor.

Analyzing the results together, the addition of only 0.5% w/w of MMT was effective to improve the film properties, in addition to showing hydrophilic behavior as pear surface. Thus, that was the optimal treatment chosen to initiate the preliminary coating tests.

The coating of the fruits happened successfully, with no cracks or bubbles being noticed. After 15 days of storage, it was observed an increase of weight loss for pears without coating while coated ones (CH and MMT) showed less loss. Preliminarily, comparing CH and MMT-0.5, the best result obtained was for MMT -0.5 which is consistent with the WVPR presented for this film since it is related to the loss of water vapor through transpiration. However, only the reduction in weight loss is not an indication of an increase of fruits shelf life and further analysis must be conducted to verify the maintenance of the pear quality during storage.

Nevertheless, it can be concluded that it was possible to obtain a nanocomposite that met the objective required. The nanocomposite composed of CH and 0.5% w/w MMT showed an improvement of its barrier and mechanical properties, and it was possible to elucidate its structure. In the preliminary coating tests of Williams pears, MMT-0.5 was demonstrated to be a potential candidate for application as fruits coating, but further investigation for its use is obligatory.

ACKNOWLEDGEMENTS

The authors would like to thank Embrapa Instrumentação (Brazil) for the collaboration with this research and the Coordenação de Aperfeiçoamento de Pessoal de Nível Superior – Brasil (CAPES) for funding part of this work.

DECLARATION OF CONFLICTING INTERESTS

The author(s) declared no potential conflicts of interest with respect to the research, authorship, and/or publication of this article.

FUNDING

The author(s) disclosed receipt of the following financial support for the research, authorship, and/or publication of this article: This work was supported in part by Coordenação de Aperfeiçoamento de Pessoal de Nível Superior – Brasil (CAPES) – Finance Code 001.

ORCID iDs

Camilly Aparecida Reis  <https://orcid.org/0000-0003-0211-9841>

Lívia Elisabeth Vasconcellos de Siqueira Brandão Vaz  <https://orcid.org/0000-0002-7444-8102>

REFERENCES

- Ahmed T, Noman M, Luo J, et al. (2021). Bioengineered chitosan-magnesium nanocomposite: A novel agricultural antimicrobial agent against *Acidovorax oryzae* and *rhizoctonia solani* for sustainable rice production. *International Journal of Biological Macromolecules* 168: 834–845. DOI: 10.1016/j.ijbiomac.2020.11.148. Elsevier B.V.
- Alexandre M and Dubois P. (2000). Polymer-layered silicate nanocomposites: Preparation, properties and uses of a new class of materials. *Materials Science and Engineering R: Reports* 28(1): 1–63. DOI: 10.1016/S0927-796X(00)00012-7. Elsevier.
- Ali S, Anjum MA, Ejaz S, et al. (2021). Carboxymethyl cellulose coating delays chilling injury development and maintains eating quality of ‘kinnow’ mandarin fruits during low temperature storage. *International Journal of Biological Macromolecules* 168: 77–85. DOI: 10.1016/j.ijbiomac.2020.12.028. Elsevier B.V.
- Aman Mohammadi M, Ramezani S, Hosseini H, et al. (2021). Electrospun antibacterial and antioxidant zein/poly(lactic acid)/hydroxypropyl methylcellulose nanofibers as an active food packaging system. *Food and Bioprocess Technology* 14: 1529–1541. DOI: 10.1007/s11947-021-02654-7. Springer.
- Amor G, Sabbah M, Caputo L, et al. (2021). Basil essential oil: Composition, antimicrobial properties, and microencapsulation to produce active chitosan films for food packaging. *Foods (Basel, Switzerland)* 10(1): 121. DOI: 10.3390/foods10010121. MDPI AG.
- Anusha JR, Fleming AT, Valan Arasu M, et al. (2016). Mechanochemical synthesis of chitosan submicron particles from the gladius of *todarodes pacificus*. *Journal of Advanced Research* 7(6): 863–871. DOI: 10.1016/j.jare.2016.08.006.
- Assis OBG and Britto Dd. (2014). Revisão: Coberturas comestíveis protetoras em frutas: Fundamentos e aplicações. *Brazilian Journal of Food Technology* 17(2): 87–97. FapUNIFESP (SciELO). DOI: 10.1590/bjft.2014.019.
- ASTM International. (2000b). ASTM E96-00, Standard test methods for water vapor transmission of materials. DOI: 10.1520/E0096-00.
- ASTM International (2000a). ASTM D882-09, Standard Test Method for Tensile Properties of Thin Plastic Sheeting. DOI: 10.1520/D0882-09.
- Beigzadeh Ghelejlou S, Esmaili M and Almasi H. (2016). Characterization of chitosan-nanoclay bionanocomposite active films containing milk thistle extract. *International Journal of Biological Macromolecules* 86: 613–621. DOI: 10.1016/j.ijbiomac.2016.02.012.
- Bensalem S, Hamdi B, Del Confetto S, et al. (2017). Characterization of chitosan/montmorillonite bionanocomposites by inverse gas chromatography. *Colloids and Surfaces A: Physicochemical and Engineering Aspects* 516: 336–344. DOI: 10.1016/j.colsurfa.2016.12.051.
- Bragg W. (1912). The diffraction of short electromagnetic waves by a crystal. *Proceedings of the Cambridge Philosophical Society* 17: 43–57.
- Bragg WH, Bragg Apr WL, Bragg BW H, et al. (1913). The reflection of X-rays by crystals. *Proceedings of the Royal Society of London. Series A, Containing Papers of a Mathematical and Physical Character* 88(605): 428–438. The Royal Society.
- Bumbudsanpharoke N, Lee W, Choi JC, et al. (2017). Influence of montmorillonite nanoclay content on the optical, thermal, mechanical, and barrier properties of low-density polyethylene. *Clays and Clay Minerals* 65(6): 387–397. Clay Minerals Society. DOI: 10.1346/CCMN.2017.064071.
- Casariago A, Souza BWS, Cerqueira MA, et al. (2009). Chitosan/clay films’ properties as affected by biopolymer and clay micro/nanoparticles’ concentrations. *Food Hydrocolloids* 23(7): 1895–1902. DOI: 10.1016/j.foodhyd.2009.02.007.
- Chen P, Xie F, Tang F, et al. (2021). Influence of plasticiser type and nanoclay on the properties of chitosan-based materials. *European Polymer Journal* 144. DOI: 10.1016/j.eurpolymj.2020.110225. Elsevier Ltd
- Chitarra M and Chitarra A. (2005). *Pós-Colheita de Frutas E Hortaliças: Fisiologia E Manuseio*, 2. ed. rev Lavras: Universidade Federal de Lavras.
- Contreras-Oliva A, Pérez-Gago MB and Rojas-Argudo C. (2012). Effects of chitosan coatings on physicochemical and nutritional quality of clementine mandarins cv. ‘oronules’. *Food Science and Technology International* 18(4): 303–315. DOI: 10.1177/1082013211427953.
- Cortez-Vega WR, Pizato S, De Souza JTA, et al. (2014). Using edible coatings from whitemouth croaker (*micropogonias furnieri*) protein isolate and organo-clay nanocomposite for improve the conservation properties of fresh-cut ‘formosa’ papaya. *Innovative Food Science and Emerging Technologies* 22: 197–202. DOI: 10.1016/j.ifset.2013.12.007. Elsevier B.V.
- Darder M, Colilla M and Ruiz-Hitzky E. (2003). Biopolymer-clay nanocomposites based on chitosan intercalated in montmorillonite. *Chemistry of Materials* 15(20): 3774–3780. American Chemical Society. DOI: 10.1021/cm0343047.
- Darder M, Colilla M and Ruiz-Hitzky E. (2005). Chitosan-clay nanocomposites: Application as electrochemical sensors. *Applied Clay Science* 28(1-4 SPEC. ISS.): 199–208. DOI: 10.1016/j.clay.2004.02.009.
- Dhall RK. (2013). Advances in edible coatings for fresh fruits and vegetables: A review. *Critical Reviews in Food Science and Nutrition. Crit Rev Food Sci Nutr* 53(5): 435–50. DOI: 10.1080/10408398.2010.541568.

- Díaz-Montes E and Castro-Muñoz R. (2021). Edible films and coatings as food-quality preservers: An overview. *Foods*. MDPI AG 10(2): 249. DOI: 10.3390/foods10020249.
- Elsabee MZ and Abdou ES. (2013). Chitosan based edible films and coatings: A review. *Materials Science and Engineering C. Mater Sci Eng C Mater Biol Appl* 33(4): 1819–1841. DOI: 10.1016/j.msec.2013.01.010.
- Fei Liu X, Lin Guan Y, Zhi Yang D, et al. (2001). Antibacterial action of chitosan and carboxymethylated chitosan. *Journal of Applied Polymer Science* 79(7): 1324–1335. DOI: 10.1002/1097-4628(20010214)79:7<1324::AID-APP210>3.0.CO;2-L. John Wiley & Sons, Ltd.
- Ferreira DF. (2015). *Sisvar*. 5.6. Lavras: Universidade Federal de Lavras, Departamento de Estatística.
- Fiori APSDM, Gabiraba VP, Praxedes APP, et al. (2014). Preparação e caracterização de nanocompósitos poliméricos baseados em quitosana e argilo minerais. *Polimeros* 24(5): 628–635. DOI: 10.1590/0104-1428.1572. Associacao Brasileira de Polimeros.
- Giannakas A, Grigoriadi K, Leontiou A, et al. (2014). Preparation, characterization, mechanical and barrier properties investigation of chitosan-clay nanocomposites. *Carbohydrate Polymers* 108(1): 103–111. DOI: 10.1016/j.carbpol.2014.03.019. Elsevier Ltd.
- Gontard N, Duchez C, Cuq J-L, et al. (1994). Edible composite films of wheat gluten and lipids: Water vapour permeability and other physical properties. *International Journal of Food Science & Technology* 29(1): 39–50. John Wiley & Sons, Ltd. DOI: 10.1111/j.1365-2621.1994.tb02045.x.
- Guimarães M, Botaro R, Novack KM, et al. (2015). Starch/PVA-based nanocomposites reinforced with bamboo nanofibrils. *Industrial Crops and Products* 70: 72–83. DOI: 10.1016/j.indcrop.2015.03.014.
- Günster E, Pestrelli D, Ünlü CH, et al. (2007). Synthesis and characterization of chitosan-MMT biocomposite systems. *Carbohydrate Polymers* 67(3): 358–365. DOI: 10.1016/j.carbpol.2006.06.004.
- Hu C, Deng Y, Hu H, et al. (2016). Adsorption and intercalation of low and medium molar mass chitosans on/in the sodium montmorillonite. *International Journal of Biological Macromolecules* 92: 1191–1196. Elsevier B.V. DOI: 10.1016/j.ijbiomac.2016.08.007.
- Jafarzadeh S, Mohammadi Nafchi A, Salehabadi A, et al. (2021). Application of bio-nanocomposite films and edible coatings for extending the shelf life of fresh fruits and vegetables. *Advances in Colloid and Interface Science* 291: 102405. DOI: 10.1016/j.cis.2021.102405. Elsevier B.V.
- Jampafuang Y, Tongta A and Waiprib Y. (2019). Impact of crystalline structural differences between α - and β -chitosan on their nanoparticle formation via ionic gelation and superoxide radical scavenging activities. *Polymers* 11(12): 2010. DOI: 10.3390/polym11122010. MDPI AG.
- Joseph SM, Krishnamoorthy S, Paranthaman R, et al. (2021). A review on source-specific chemistry, functionality, and applications of chitin and chitosan. *Carbohydrate Polymer Technologies and Applications* 2: 100036. Elsevier BV. DOI: 10.1016/j.carpta.2021.100036.
- Kasaai MR. (2009). Various methods for determination of the degree of N-acetylation of chitin and chitosan: A review. *Journal of Agricultural and Food Chemistry. J Agric Food Chem* 57(5): 1667–1676. DOI: 10.1021/jf803001m.
- Kaur S and Dhillon GS. (2014). The versatile biopolymer chitosan: Potential sources, evaluation of extraction methods and applications. *Critical Reviews in Microbiology. Crit Rev Microbiol* 40(2): 155–75. DOI: 10.3109/1040841X.2013.770385.
- Ke CL, Deng FS, Chuang CY, et al. (2021). Antimicrobial actions and applications of chitosan. *Polymers* 13(6): 904. DOI: 10.3390/polym13060904. MDPI AG.
- Klangmuang P and Sothornvit R. (2018). Active coating from hydroxypropyl methylcellulose-based nanocomposite incorporated with Thai essential oils on mango (cv. Namdokmai sithong). *Food Bioscience* 23: 9–15. Elsevier Ltd. DOI: 10.1016/j.fbio.2018.02.012.
- Kusmono and Abdurrahim I. (2019). Water sorption, antimicrobial activity, and thermal and mechanical properties of chitosan/clay/glycerol nanocomposite films. *Heliyon* 5(8): e02342. DOI: 10.1016/j.heliyon.2019.e02342. Elsevier Ltd.
- Lavorgna M, Piscitelli F, Mangiacapra P, et al. (2010). Study of the combined effect of both clay and glycerol plasticizer on the properties of chitosan films. *Carbohydrate Polymers* 82(2): 291–298. DOI: 10.1016/j.carbpol.2010.04.054.
- Li J, Yan J, Cao J, et al. (2012). Preventing the wound-induced deterioration of yali pears by chitosan coating treatments. *Food Science and Technology International* 18(2): 123–128. DOI: 10.1177/1082013211414774.
- Lim JW, Lim WS, Lee MH, et al. (2021). Barrier and structural properties of polyethylene terephthalate film coated with poly(acrylic acid)/montmorillonite nanocomposites. *Packaging Technology and Science* 34(3): 141–150. John Wiley and Sons Ltd. DOI: 10.1002/pts.2547.
- Martínez-Camacho AP, Cortez-Rocha MO, Ezquerro-Brauer JM, et al. (2010). Chitosan composite films: Thermal, structural, mechanical and antifungal properties. *Carbohydrate Polymers* 82(2): 305–315. DOI: 10.1016/j.carbpol.2010.04.069.
- Másson M. (2021). 33 - Chitin and chitosan. In: Phillips GO and Williams PA (eds) *Handbook of Hydrocolloids*. 3ed. United Kingdom: Elsevier, 1039–1072. DOI: 10.1016/B978-0-12-820104-6.00013-9.
- Merinska D, Malac Z, Pospisil M, et al. (2002). Polymer/clay nanocomposites based on MMT/ODA intercalates. *Composite Interfaces* 9: 6. Taylor & Francis Group : 529. DOI: 10.1163/15685540260494100.540.
- Mogilevskaya EL, Akopova TA, Zelenetskii AN, et al. (2006). The crystal structure of chitin and chitosan. *Polymer Science - Series A* 48(2): 116–123. Springer. DOI: 10.1134/S0965545X06020039.
- Moraes KS, Fagundes C, Melo MC, et al. (2012). Conservação de pera williams utilizando coberturas comestíveis compostas de alginato e carragena. *Ciencia e Tecnologia de Alimentos* 32(4): 679–684. Sociedade Brasileira de Ciência e Tecnologia de Alimentos. DOI: 10.1590/S0101-20612012005000106.
- Nagarajan M, Benjakul S, Prodpran T, et al. (2014). Characteristics of bio-nanocomposite films from tilapia skin gelatin incorporated with hydrophilic and hydrophobic nanoclays. *Journal of Food Engineering* 143: 195–204. Elsevier Ltd. DOI: 10.1016/j.jfoodeng.2014.06.038.

- Naqash F, Masoodi FA, Ayob O, et al. (2021). Effect of active pectin edible coatings on the safety and quality of fresh-cut apple. *International Journal of Food Science and Technology*. DOI: 10.1111/ijfs.15059. Blackwell Publishing Ltd
- Ojeda GA, Arias Gorman AM, Sgroppo SC, et al. (2021). Application of composite cassava starch/chitosan edible coating to extend the shelf life of black mulberries. *Journal of Food Processing and Preservation* 45: e15073. DOI: 10.1111/jfpp.15073. Blackwell Publishing Ltd.
- Otoni CG, Avena-Bustillos RJ, Azeredo HMC, et al. (2017). Recent advances on edible films based on fruits and vegetables—A review. *Comprehensive Reviews in Food Science and Food Safety* 16(5): 1151–1169. Blackwell Publishing Inc. DOI: 10.1111/1541-4337.12281.
- Özdemir KS and Gökmen V. (2017). Extending the shelf-life of pomegranate arils with chitosan-ascorbic acid coating. *LWT - Food Science and Technology* 76(Part A): 172–180. DOI: 10.1016/j.lwt.2016.10.057.
- Paiva Ld, Morales AR and Díaz FRV (2008) Argilas organofílicas: características, metodologias de preparação, compostos de intercalação e técnicas de caracterização. *Cerâmica* 54(330). DOI: 10.1590/S0366-69132008000200012.
- Panahirad S, Naghshiband-Hassani R and Mahna N. (2020). Pectin-based edible coating preserves antioxidative capacity of plum fruit during shelf life. *Food Science and Technology International* 26(7): 583–592. DOI: 10.1177/1082013220916559.
- Pandey JK, Pratheep Kumar A, Misra M, et al. (2005). Recent advances in biodegradable nanocomposites. *Journal of Nanoscience and Nanotechnology* 5(4): 497–526. DOI: 10.1166/jnn.2005.111.
- Pandey S and Mishra SB. (2011). Organic-inorganic hybrid of chitosan/organoclay bionanocomposites for hexavalent chromium uptake. *Journal of Colloid and Interface Science* 361(2): 509–520. DOI: 10.1016/j.jcis.2011.05.031.
- Pavlidou S and Papispyrides CD. (2008). A review on polymer-layered silicate nanocomposites. *Progress in Polymer Science (Oxford)* 33(12): 119–1198. DOI: 10.1016/j.progpolymsci.2008.07.008.
- Pereira FAR, Sousa KS, Cavalcanti GRS, et al. (2017). Green biosorbents based on chitosan-montmorillonite beads for anionic dye removal. *Journal of Environmental Chemical Engineering* 5(4): 3309–3318. DOI: 10.1016/j.jece.2017.06.032.
- Pinto AMB, Santos TM, Caceres CA, et al. (2015). Starch-cashew tree gum nanocomposite films and their application for coating cashew nuts. *LWT - Food Science and Technology* 62(1): 549–554. DOI: 10.1016/j.lwt.2014.07.028.
- Pires JRA, Souza Vd and Fernando AL. (2018). Chitosan/montmorillonite bionanocomposites incorporated with rosemary and ginger essential oil as packaging for fresh poultry meat. *Food Packaging and Shelf Life* 17: 142–149. Elsevier BV. DOI: 10.1016/j.fpsl.2018.06.011.
- Pranoto Y, Rakshit SK and Salokhe VM. (2005). Enhancing antimicrobial activity of chitosan films by incorporating garlic oil, potassium sorbate and nisin. *LWT - Food Science and Technology* 38(8): 859–865. Academic Press. DOI: 10.1016/j.lwt.2004.09.014.
- Priyadarshi R, Kim SM and Rhim JW. (2021). Pectin/pullulan blend films for food packaging: Effect of blending ratio. *Food Chemistry* 347: 129022. DOI: 10.1016/j.foodchem.2021.129022. Elsevier Ltd.
- Ramadan AR, Esawi AMK and Gawad AA. (2010). Effect of ball milling on the structure of Na⁺-montmorillonite and organo-montmorillonite (Cloisite 30B). *Applied Clay Science* 47(3–4): 196–202. DOI: 10.1016/j.clay.2009.10.002.
- Rhim JW. (2011). Effect of clay contents on mechanical and water vapor barrier properties of agar-based nanocomposite films. *Carbohydrate Polymers* 86(2): 691–699. Elsevier. DOI: 10.1016/j.carbpol.2011.05.010.
- Rhim JW, Hong SI, Park HM, et al. (2006). Preparation and characterization of chitosan-based nanocomposite films with antimicrobial activity. *Journal of Agricultural and Food Chemistry* 54(16): 5814–5822. J Agric Food Chem. DOI: 10.1021/jf060658h.
- Riaz A, Aadil RM, Amoussa AMO, et al. (2021). Application of chitosan-based apple peel polyphenols edible coating on the preservation of strawberry (*Fragaria ananassa* cv hongyan) fruit. *Journal of Food Processing and Preservation* 45: e15018. DOI: 10.1111/jfpp.15018. Blackwell Publishing Ltd.
- Rohini B, Padma Ishwarya S, Rajasekharan R, et al. (2020). *Ocimum basilicum* seed mucilage reinforced with montmorillonite for preparation of bionanocomposite film for food packaging applications. *Polymer Testing* 87: 106465. Elsevier Ltd. DOI: 10.1016/j.polymertesting.2020.106465.
- Santos OS. (1989). *Ciência E Tecnologia de Argilas*, 2 ed São Paulo: Edgard Blucher.
- Silvestre C, Duraccio D and Cimmino S. (2011). Food packaging based on polymer nanomaterials. *Progress in Polymer Science (Oxford)* 36(12): 1766–1782. DOI: 10.1016/j.progpolymsci.2011.02.003. Elsevier Ltd.
- Sousa FF, Pinsetta Junior JS, Oliveira KTEF, et al. (2021). Conservation of ‘palmer’ mango with an edible coating of hydroxypropyl methylcellulose and beeswax. *Food Chemistry* 346: 128925. DOI: 10.1016/j.foodchem.2020.128925. Elsevier Ltd.
- Souza VGL, Pires JRA, Rodrigues PF, et al. (2018). Bionanocomposites of chitosan/montmorillonite incorporated with *Rosmarinus officinalis* essential oil: Development and physical characterization. *Food Packaging and Shelf Life* 16: 148–156. Elsevier Ltd. DOI: 10.1016/j.fpsl.2018.03.009.
- Souza VGL, Pires JRA, Vieira ÉT, et al. (2019). Activity of chitosan-montmorillonite bionanocomposites incorporated with rosemary essential oil: From in vitro assays to application in fresh poultry meat. *Food Hydrocolloids* 89: 241–252. Elsevier B.V. DOI: 10.1016/j.foodhyd.2018.10.049.
- Sultan M, Hafez OM, Saleh MA, et al. (2021). Smart edible coating films based on chitosan and beeswax-pollen grains for the postharvest preservation of Le conte pear. *RSC Advances* 11(16): 9572–9585. Royal Society of Chemistry. DOI: 10.1039/D0RA10671B.
- Tetens VO. (1930). Über einige meteorologische begriffe. *Z-Geophysik* 6: 297–309. <https://ci.nii.ac.jp/naid/10003553214/en/>
- Van Den Broek LAM, Knoop RJI, Kappen FHJ, et al. (2015). Chitosan films and blends for packaging material. *Carbohydrate Polymers* 116: 237–242. Elsevier Ltd. DOI: 10.1016/j.carbpol.2014.07.039.

- Vieira ACF, de Matos Fonseca J, Menezes NMC, et al. (2020). Active coatings based on hydroxypropyl methylcellulose and silver nanoparticles to extend the papaya (*Carica papaya* L.) shelf life. *International Journal of Biological Macromolecules* 164: 489–498. Elsevier B.V. DOI: 10.1016/j.ijbiomac.2020.07.13.
- Vieira JM, Flores-López ML, Rodríguez DJ, et al. (2016). Effect of chitosan-Aloe vera coating on postharvest quality of blueberry (*Vaccinium corymbosum*) fruit. *Postharvest Biology and Technology* 116: 88–97. DOI: 10.1016/j.postharvbio.2016.01.011.
- Vlacha M, Giannakas A, Katapodis P, et al. (2016). On the efficiency of oleic acid as plasticizer of chitosan/clay nanocomposites and its role on thermo-mechanical, barrier and antimicrobial properties - comparison with glycerol. *Food Hydrocolloids* 57: 10–19. Elsevier. DOI: 10.1016/j.foodhyd.2016.01.003.
- Wang SF, Shen L, Tong YJ, et al. (2005). Biopolymer chitosan/montmorillonite nanocomposites: Preparation and characterization. *Polymer Degradation and Stability* 90(1): 123–131. DOI: 10.1016/j.polymdegradstab.2005.03.001.
- Wang X, Du Y and Luo J. (2008). Biopolymer/montmorillonite nanocomposite: Preparation, drug-controlled release property and cytotoxicity. *Nanotechnology* 19(6): 065707. DOI: 10.1088/0957-4484/19/6/065707. Nanotechnology.
- Xu D, Qin H and Ren D. (2018). Prolonged preservation of tangerine fruits using chitosan/montmorillonite composite coating. *Postharvest Biology and Technology* 143: 50–57. Elsevier B.V. DOI: 10.1016/j.postharvbio.2018.04.013.
- Yan W, Chen W, Muhammad U, et al. (2019). Preparation of α -tocopherol-chitosan nanoparticles/chitosan/montmorillonite film and the antioxidant efficiency on sliced dry-cured ham. *Food Control* 104: 132–138. Elsevier Ltd. DOI: 10.1016/j.foodcont.2019.04.026.
- Yaradoddi JS, Banapurmath NR, Ganachari S V, et al. (2020). Biodegradable carboxymethyl cellulose based material for sustainable packaging application. *Scientific Reports* 10: 21960. DOI: 10.1038/s41598-020-78912-z. Nature Research.
- Zambrano-Zaragoza ML, González-Reza R, Mendoza-Muñoz N, et al. (2018). Nanosystems in edible coatings: A novel strategy for food preservation. *International Journal of Molecular Sciences* 19(3): 705. DOI: 10.3390/ijms19030705. MDPI AG.
- Zeng QH, Yu AB, Lu GQ, et al. (2005). Clay-based polymer nanocomposites: Research and commercial development. *Journal of Nanoscience and Nanotechnology* 5(10): 1574–1592. DOI: 10.1166/jnn.2005.411.
- Zhang Y, Xue C, Xue Y, et al. (2005). Determination of the degree of deacetylation of chitin and chitosan by X-ray powder diffraction. *Carbohydrate Research* 340(11): 1914–1917. DOI: 10.1016/j.carres.2005.05.005.
- Zhou W, He Y, Liu F, et al. (2021). Carboxymethyl chitosan-pullulan edible films enriched with galangal essential oil: Characterization and application in mango preservation. *Carbohydrate Polymers* 256: 117579. DOI: 10.1016/j.carbpol.2020.117579. Elsevier Ltd.
- Zubair M, Pradhan RA, Arshad M, et al. (2021). Recent advances in lipid derived Bio-based materials for food packaging applications. *Macromolecular Materials and Engineering* 2000799: 2000799. DOI: 10.1002/mame.202000799.